Materials Science & Engineering A 711 (2018) 149–155

Contents lists available at ScienceDirect

Materials Science & Engineering A

journal homepage: www.elsevier.com/locate/msea

Crystallographic texture and lattice strain evolution during tensile load of swaged brass

Nowfal Al-Hamdany[a,*], Heinz-Günter Brokmeier[a], Weimin Gan[b]

[a] Institut für Werkstoffkunde und Werkstofftechnik, TU Clausthal, Agricolastr. 6, D-38678 Clausthal-Zellerfeld, Germany
[b] German Engineering Materials Science Center at MLZ, Helmholtz-Zentrum Geesthacht, D-85748 Garching, Germany

ARTICLE INFO

Keywords:
Crystallographic texture
Lattice strain
Swaging
Brass
Neutrons diffractions

ABSTRACT

Evolutions of texture and lattice strain of swaged brass samples were investigated by neutron diffraction at STRESS-SPEC under tensile deformation using a unique tension/compression rig. The two phased sample BS1 (61% α-brass and 39% β-brass) became 100% α-brass after 400 °C annealing (sample BS2). The starting texture of the as-received material BS1 was the typical < 111 >, < 200 > double fiber. This texture develops firstly by in-situ tension to a moderate strengthening. After annealing (BS2) the < 111 > fiber survives with surprisingly high strength and develops by in-situ tension a very strong < 111 > fiber of 39 mrd. Line broadening and lattice strain behaviour shows the development of the elastic strain and plastic strain.

1. Introduction

Swaging is a highly used manufacturing process to improve materials properties, such as fatigue behaviour, strength and corrosion properties. Different types of swaging are in use, which is basically forging. Most of the swaging types are ideal for mass production. One in particular, rotary swaging (Fig. 1) can be used to reduce the cross section of rods and tubes and also to increase the strength [1]. An example of this type of swaging can be applied to the weight reduction of bike axles or high pressure tubes. The property change after swaging is based on grain refinement, strengthening of the crystallographic texture and generation of compressive stresses on the surface. It should be noted that most swaging processes are cold working processes, which reduces the costs.

Rotary swaging in ideal conditions belongs to uniaxial deformation, same as wire and rod drawing. Uniaxial deformation is known for the high texture symmetry, which is defined by ideal fiber texture with a preferred fiber axis in transport direction and a rotational freedom around this fiber axis [2,3]. From Fig. 1, it can be deduced that due to the forging matrix which can consist of 2, 3, 4 or 6 segments a little variation from the ideal fiber texture can be observed.

The texture symmetry is related to the process but the fiber type depends on the crystal symmetry and also on the stacking fault energy of the swaged material. FCC metals typically develop double fibers of < 111 > and < 100 > under uniaxial tension. The ratio depends on the stacking fault energy [2,3]. BCC metals show typically a < 110 > fiber [2,3]. HCP metals tend to have either the < 10.0 > or the < 11.0 > fiber sometimes a double fiber < 10.0 >, < 11.0 > generates. A mixture of materials in case of precipitations or composites needs a co-deformation during swaging. In general it is known that a second phase influences texture development during deformation and recrystallization often in a decrease of the texture sharpness as well as the final mechanical properties [4].

Neutron diffraction allows the texture determination of the average texture over the whole cross section of rotary swaged samples, which is ideal for technical applications. This is possible because of the high penetration power of neutrons against standard X-rays. Moreover, the possibility to get complete pole figures makes the error of texture sharpness low, so that the expected variations in texture sharpness can be obtained in high quality [5–7].

Kalu et al. [8] have investigated the texture evolution in swaged Cu wire and Cu-Nb/Ti composite. Both materials developed < 111 > and < 100 > fiber texture. Cu-Nb/Ti composite had generally less texture sharpness than those of pure Cu. Hupalo et al. [9] have studied the evolution of texture and microstructure during cold swaging and recrystallization of Oligocrystalline INCOLOY® MA 956. They have used light optical microscopy, transmission electron microscopy, X-ray diffraction, electron back scattered diffraction (EBSD) and Vickers microhardness testing. A sharp < 110 > fiber texture was developed during plastic deformation after starting from a strong < 111 > fiber. They observed that recrystallization did not change the texture significantly. Gue et al. [10] have evaluated the texture during recrystallization of cold swaged Ti-Nb-Ta-Zr-O alloy (TNTZO). The texture measurements showed a pronounced < 110 > fiber along the

* Corresponding author.
E-mail address: nowfal.alhamdany@tu-clausthal.de (N. Al-Hamdany).

https://doi.org/10.1016/j.msea.2017.11.047
Received 15 June 2017; Received in revised form 2 November 2017; Accepted 13 November 2017
Available online 14 November 2017
0921-5093/

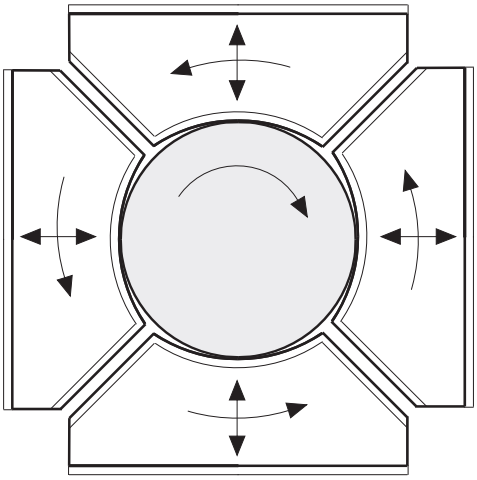

Fig. 1. Scheme of the swaging process with 4 segments.

deformation axis in the cold swaged TNTZO alloy which is the typical fiber texture for bcc materials after drawing or swaging. The < 110 > fiber texture was gradually replaced by random orientations by increasing the annealing time. Gan et al. [11,12] have investigated the bulk and local texture evolution of pure Mg processed by rotary swaging. They started from diameter of 10 mm going down to 4.5 mm which is corresponding to a deformation degree of 1.58. A main {00.2} basal fiber texture in rotary swaging processed Mg was observed. Basal planes tend to be more homogeneous with the increase of the process pass. Texture was relatively inhomogeneous from the surface to the center at rods which indicate a non-uniform deformation. Bache et al. [13] have characterized an advanced Nickel based superalloy RR1000 post cold work by swaging. Cold work of 30% was subjected to cylindrical bars of 27 mm diameter. Beside the reduction in grain size, a relatively strong < 111 > fiber texture parallel to the longitudinal bar axis has been confirmed by EBSD. The effect of cold work on bulk mechanical properties was observed from the increase in the ultimate tensile strength (UTS) and yield tensile strength (YTS), but also resulted in reduced ductility. The ductility reduced between room temperature and 500 °C before the ductility then recovered at higher temperatures.

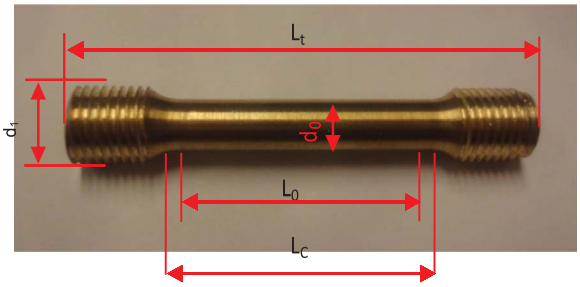

Fig. 3. Dimensions of the brass tensile sample.

STRESS-SPEC is equipped with a tensile/compression machine having a rotated rig (χ tilt and ϕ rotation) with a maximum load of 50 kN. Different sample geometries are possible to be measured by this machine. An additional light furnace can be installed around the loaded sample with temperature up to 1000 °C [14,15].

Commercial Cu-36%Zn brass (Fig. 2) was chosen firstly due to expected activation of deformation twins during deformation and secondly because of the mixture of α- and β-brass. This alloy has excellent cold workability. Typical applications of Cu-36%Zn are radiator cores, tanks, lamp fixtures, fasteners, locks, hinges, plumbing accessories, pins, rivets [16].

The aim of this experiment was to investigate the influence of the existing preferred orientation on texture development of α brass during tensile load for α + β brass and α brass. Additionally, the evolution of line broadening (defect evolution) and line position (lattice strain) of both samples BS1 and BS2 were investigated during tensile loading.

2. Materials and experimental procedure

Two samples were produced from commercial Cu-36%Zn brass. One sample (BS1) was swaged up to a deformation degree of φ = 3 having a reduction in cross section from 32 mm in diameter to 7 mm. Sample 2 (BS2) was additionally annealed for 2 h at 400 °C after swaging. During this annealing β-brass was solved and BS2 consists only of α-brass. Phase analysis was carried out with hard X-rays at the high energy beamline HEMS@Petra III. The microstructure was examined for both

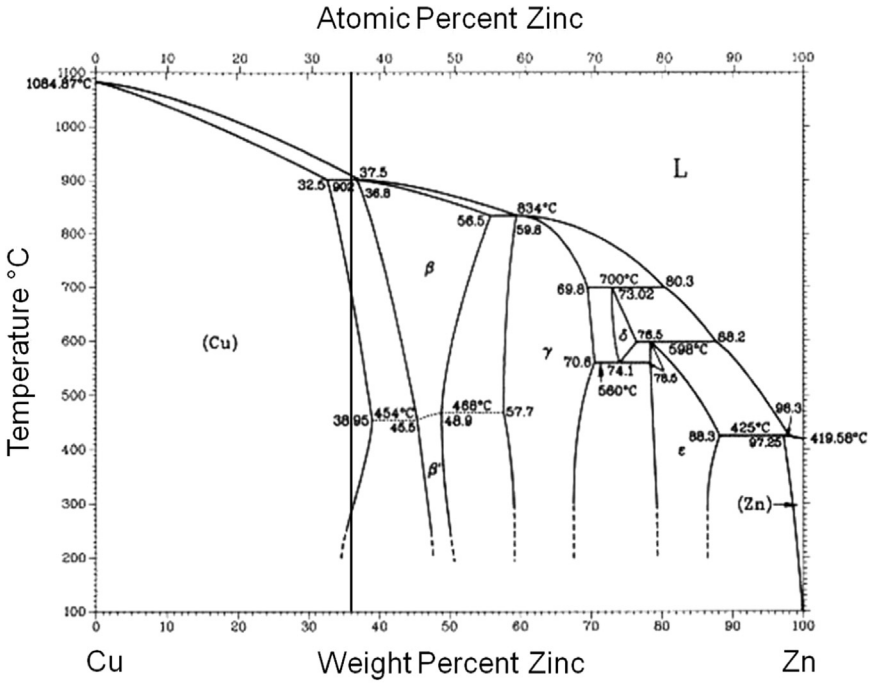

Fig. 2. Phase diagram of Cu-Zn alloy [17].